Unraveling the Missing Link in Low-power Communication: An Autodyning Receiver Architecture that Achieves a Long Range

Sooriya Patabandige Pramuka Medaranga
National University of Singapore
pramuka@u.nus.edu

Rajashekar Reddy Chinthalapani
National University of Singapore
rajashekar.c@u.nus.edu

Wenqing Yan*
Uppsala University
wenqing.yan@it.uu.se

Prabal Dutta
UC Berkeley
prabal@berkeley.edu

Ambuj Varshney
National University of Singapore
ambujv@nus.edu.sg

Abstract

Wireless communication remains the most power-intensive operation in embedded systems. Decades of research have enabled radio transmitters to operate at power levels as low as tens of µWs while maintaining practical communication ranges. However, achieving power-efficient reception over similarly useful distances has received *significantly* less attention. State-of-the-art low-power receivers typically rely on Schottky diode-based envelope detectors, which are inherently limited in sensitivity and unable to support complex modulation schemes. We introduce SoMix, the *Single Oscillator Mixer* receiver, a novel architecture that uses tunnel diode oscillators to overcome these limitations. Specifically, we demonstrate the *autodyning* property of tunnel diode oscillators, allowing a single circuit to generate both a carrier signal and perform signal downconversion, thus merging two traditionally power-hungry analog tasks into one energy-efficient step. The SoMix front-end consumes less than 100 µW while supporting high-sensitivity reception. Through injection-locking, SoMix stabilizes its tunnel diode oscillator using even a weak external carrier signal, allowing it to receive frequency-modulated transmissions from distances greater than 100 meters in line-of-sight environments. We also demonstrate that the SoMix exhibits robustness in complex real-world scenarios. SoMix outperforms state-of-the-art receivers in power, range, and functionality.

CCS Concepts

• **Hardware → Sensor devices and platforms**; **Wireless devices**; *Networking hardware*; • **Computer systems organization → Sensor networks**.

Keywords

Embedded systems, backscatter, sensors, tunnel diodes, receivers

ACM Reference Format:
Sooriya Patabandige Pramuka Medaranga, Rajashekar Reddy Chinthalapani, Wenqing Yan, Prabal Dutta, and Ambuj Varshney. 2025. Unraveling the Missing Link in Low-power Communication: An Autodyning Receiver Architecture that Achieves a Long Range. In *The 23rd Annual International Conference on Mobile Systems, Applications and Services (MobiSys '25), June 23–27, 2025, Anaheim, CA, USA.* ACM, New York, NY, USA, 14 pages. https://doi.org/10.1145/3711875.3729164

*Contributed to this work while visiting the National University of Singapore.

MobiSys '25, Anaheim, CA, USA

ACM ISBN 979-8-4007-1453-5/2025/06
https://doi.org/10.1145/3711875.3729164

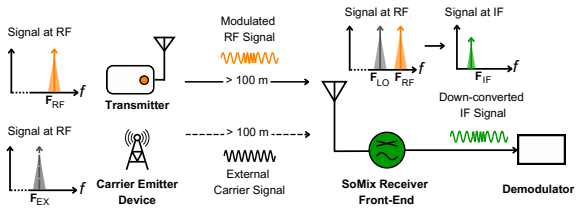

Figure 1: SoMix uses the autodyning property of the tunnel diode oscillator to receive frequency-modulated signals at distances exceeding 100 m from the transmitter. To enhance the stability of the tunnel diode oscillator, SoMix uses a carrier signal for injection-locking. The receiver can also be positioned more than 100 m away from the carrier emitter device in a line-of-sight environment. The SoMix front-end operates at a power consumption below 100 µW.

1 Introduction

Wireless communication consumes significantly more power than sensing and processing in embedded systems [1–5]. This disparity leads to frequent battery replacements [6], increased maintenance efforts, and higher deployment costs [7]. Consequently, significant efforts have been made to mitigate this challenge, focusing on improving the power efficiency of radio transmitters [3, 8–14].

Early efforts to mitigate the power challenge resulted in the design of radio duty cycle mechanisms [15–19], which aimed to maximize the inactive period of transceivers. Recent approaches reduce transmitters' active power through the backscatter mechanism. Today, after decades of effort, state-of-the-art (SoTA) backscatter transmitters achieve a power consumption comparable to sensing and processing, even while adhering to standard protocols [9, 10, 12, 20].

Communication involves both transmission *and* reception, yet the challenge of improving receiver power efficiency while maintaining a practical range for embedded applications remains largely unaddressed. Several factors contribute to this gap. *First*, classical embedded applications focus primarily on sense and transmit [6, 21], leading to extensive research on power-efficient transmitters. However, this emphasis is increasingly misaligned with the needs of emerging devices such as earphones [22] and mixed reality headsets [23–25], which rely heavily on reception. *Second*, receiver architectures are inherently complex, comprising multiple stages of analog circuits. Unlike digital components, analog circuits have not experienced significant improvements in power efficiency [26–28].

Additionally, decoupling digital and analog components has enabled power-efficient backscatter designs for transmitters, but receivers have lacked similar breakthroughs due to fundamental challenges of separating analog circuits from the receiver architecture.

Let us examine a receiver architecture. Incoming radio waves are captured by the antenna and amplified through a low-noise amplifier (LNA). The amplified signal then undergoes downconversion via a mixer, where a high-frequency oscillator generates a reference signal. This process, known as heterodyning, produces an intermediate frequency (IF) signal. The IF signal is further amplified and processed to extract the baseband signal, which contains the transmitted information. Finally, an analog-to-digital converter (ADC) digitizes the baseband signal. Each stage relies on analog circuitry, which consumes a significant amount of power [29, 30].

We introduce SoMix, a rethinking of the receiver architecture that consolidates multiple analog stages into a single step, while allowing the offloading of energy-intensive operations to external infrastructure. This is made possible by using a tunnel diode oscillator (TDO), which we demonstrate exhibits an autodyning property, central to the design of the SoMix. This property enables SoMix to achieve signal reception at distances greater than 100 m in line-of-sight from both the transmitter and the carrier emitter device (CED), representing at least an order-of-magnitude improvement over SoTA. Figure 1 provides an overview of a deployment with SoMix.

Design. The SoMix receiver is built around the use of a tunnel diode. A tunnel diode, with its heavily doped P-N junction, exhibits a region of negative resistance (RNR) due to quantum tunneling. This effect occurs at low voltages and currents, resulting in biasing power consumption on the order of tens of μW [31]. Furthermore, tunnel diodes are well-suited for operation at radio frequency (RF) frequencies. Using these unique properties, recent efforts have explored the design of low-power communication mechanisms [11, 32–35]. SoMix builds on these efforts to conceptualize a low-power receiver architecture. Let us examine the steps performed by SoMix.

The first step in a receiver involves converting incoming radio waves into electrical signals using an antenna. In conventional receivers, these signals are then amplified by an LNA to ensure sufficient strength for subsequent mixing and downconversion stages. Since LNAs operate at RF, they tend to be power-intensive. To avoid this, receivers—such as those based on envelope detectors—bypass the LNA stage and instead use Schottky diodes for rectification. However, it limits receiver sensitivity, requiring strong signals (approx. −54 dBm) due to the physical limitations of the diodes [36].

SoMix uses tunnel diodes, which offer a favourable trade-off between conventional LNA-based designs and Schottky diode-based receivers. Tunnel diodes are receptive to much weaker signals, enabling the detection of signals below the threshold detectable by Schottky-based envelope detectors, even without any amplification stage. Their biasing power-consumption is in tens of μWs. This enhanced sensitivity makes them particularly suitable for scenarios involving inherently weak signals, such as GPS reception [37], or for long-range communication, which is the motivation behind SoMix.

The receiver must convert the signal to an IF or baseband signal. Envelope detectors typically do not perform downconversion. In conventional receivers, this step involves mixing the incoming signal with a locally generated carrier signal using a mixer. In SoMix, we configure the TDO to function as both the local oscillator (LO) and the mixer. However, to achieve low power consumption, we trade-off TDO stability, resulting in a noisy carrier signal prone to drift [11, 38]. To mitigate this, we delegate the task of stabilizing the TDO to the infrastructure using the injection-locking phenomenon [11]. When two oscillators operate at similar frequencies, they can injection-lock and synchronize to a common frequency [39]. In SoMix, commodity devices generate a carrier signal that injection-locks and stabilizes the TDO, significantly improving its phase noise and frequency stability. Due to the high sensitivity of the tunnel diodes, injection locking is possible even when the CED is placed at a substantial distance (exceeding 100 m) from the receiver SoMix, ensuring a stable and precise LO for the downconversion process.

System	Radio	External Carrier (dBm)	Bitrate (bps)	Sensitivity (dBm)	Prototype	Power Draw (μW)	EPB (nJ/bit)
SoMix * (2025)	OOK/FSK	-70	up to 10K	-70	PCB	250	25.0
μMote (2023) [40]	LoRa	-48 /-43	1K /5K	-48 /-43	PCB	62	62.0 /12.4
passiveDSSS (2022) [40, 41]	DSSS	-46	1K	-46	PCB	395	395.0
Saiyan (2022) [40, 42]	LoRa	-	1K	-43 /-86	PCB /IC Simu	466 /93	466.0 /93.0
MIXIQ (2021) [29]	WiFi	-52	1125K	-52	PCB	365	0.3
802.15.4 Rx (2018) [43]	802.15.4	-7 /-14	250K	-8 /-48	IC Simu /IC Simu IF amp	286 /361	1.1 /1.4
BLE Rx (2017) [44]	BLE	3	1M	-8	PCB	-	-
WISP5 ED (2017) [44]	OOK	-	1K	-28	PCB	787	787.0
WuRx IC ED (2025) [45]	OOK	-	10K	-104	65nm CMOS IC	225	22.5
WuRx IC ED (2018) [46]	OOK	-	63K	-72	14nm CMOS IC	95	1.5
WuRx IC ED (2017) [47]	2FSK	-	31.3K	-72	65nm CMOS IC	335	10.7
WuRx IC ED (2016) [48]	OOK	-	10K	-97	65nm CMOS IC	99	9.9
WuRx IC ED (2014) [49]	OOK	-	1K /100K	-86	90nm CMOS IC	64 /146	64.0 /1.5

Table 1: ***Bit rate, receiver sensitivity, power draw and energy per bit of SOTA radios. SoMix achieves high-sensitivity due to the tunnel diode's ability to receive a significantly weaker signal than a Schottky diode.***

The stabilized carrier signal from the TDO must be mixed with an incoming signal to perform downconversion and generate an IF signal. Typically, this process requires power-intensive mixers, and handling weak signals poses additional challenges. Due to its nonlinearity, we demonstrate that the TDO can perform downconversion to an IF signal. This process, known as *autodyning*, enables a single circuit to generate both the carrier signal and the downconversion. This reduces the power consumption and complexity of the SoMix.

The IF signal may require amplification prior to digitization. To address this, we systematically examine the trade-offs between gain and power consumption and design an optional IF amplification stage that provides high gain while maintaining low-power consumption. The final step involves digitizing the IF signal, for which we implement a thresholding circuit that transforms Frequency Shift Keying (FSK) signals into amplitude-modulated signals, enabling recovery of the transmitted information. Together, SoMix achieves a sensitivity improvement of approximately 20 dB over conventional Schottky diode-based designs, as summarized in Table 1.

- The SoMix downconverts signals received from transmitters that are located up to 54m away in complex non-line-of-sight (NLoS) environments and more than 100m in line-of-sight (LoS) environments.
- SoMix can function without an emitter device, when a transmitter provides an unsuppressed carrier. Under these conditions, it achieves a range of more than 100m in a LOS environment.

2 Background

We provide background relevant for SoMix and contextualize it with previous work. We start with discussion on receiver architecture.

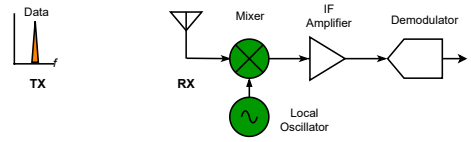

(a) Heterodyne Architecture

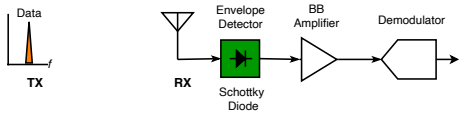

(b) Vanilla Envelope-detector Architecture

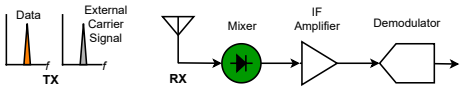

(c) External Local-oscillator Architecture

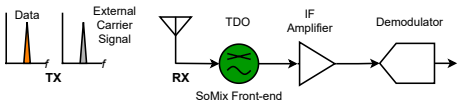

(d) SoMix Architecture

Figure 2: (a) Conventional receivers use a heterodyne architecture that relies on multiple energy-intensive analog stages. (b) Vanilla envelope detectors remove these analog stages by using Schottky diode-based rectifiers to extract the amplitude of received signals, but they suffer from poor sensitivity and cannot support complex modulation. (c) External local-oscillator receivers improve upon envelope detectors by enabling complex modulation, but they require proximity to the CED and still offer poor sensitivity. (d) SoMix introduces an autodyne architecture that replaces these complex analog stages with a single, energy-efficient stage implemented using a TDO.

Receiver architecture. A super-heterodyne receiver employs a pipelined architecture, as illustrated in Figure 2a. The receiver's analog front-end begins with a bandpass filter, eliminating out-of-band signals. This is followed by an LNA to improve the strength of the incident signal. The amplified signal is fed into a three-port mixer, where a local-oscillator provides the second input, and the output is taken from the third port. The mixer performs downconversion by combining the received signal with the high-frequency local-oscillator signal, producing an IF signal. Finally, the IF signal is digitized and processed for baseband extraction. The analog front-end, particularly the mixers and oscillators, results in high power consumption, which we address by using tunnel diodes.

Envelope detectors. Efforts to allow low-power reception focus heavily on envelope detector designs. An envelope detector consists of an antenna that is matched and connected to a diode-based rectifier, which converts incoming radio waves into electrical signals. Often, the signal undergoes further amplification through charge-doubling topologies such as the Dickson charge pump [50], Cockcroft-Walton multipliers. This approach tracks the energy of the incoming signal by extracting its amplitude. Next, this rectified signal is digitized using a thresholding circuit designed using comparators (akin to 1-bit ADC). Therefore, envelope detectors eliminate the energy-intensive steps of a conventional receiver architecture, as shown in Figure 2b.

Although envelope detectors are passive, they have limitations. The Schottky diode exhibits poor sensitivity, making it challenging to extract weak signals (-54 dBm). Furthermore, envelope detectors cannot perform the downconversion required to extract the IF signal. As a result, they can only support simple modulation schemes, such as On-Off Keying (OOK), as they cannot capture phase and frequency information from the received signal. In contrast, state-of-the-art low-power transmitters often employ complex modulation techniques to achieve higher data rates [9, 51]. This mismatch makes envelope detector-based receivers a bottleneck, limiting the overall communication capabilities of the embedded system.

Enhanced envelope detectors and Wake-up receivers. Recent efforts have extended the use of envelope detectors to support the reception of FSK [47] and chirp spread spectrum (CSS) signals [42]. However, they remain limited by their reliance on extracting and amplifying only the signal envelope, which prevents them from utilizing IF signals and fully supporting complex modulation schemes.

The envelope detectors form the basis for Wake-up Receiver (WuRx). As shown by the performance listed in Table 1, their sensitivity can be improved from -72 dBm to -104 dBm by incorporating IF amplification stages. Due to the power efficiency of the integrated circuits, the WuRx receivers operate at a power consumption of less than 100 µW. However, this combination of low-power consumption and high sensitivity often comes at the cost of a limited bit rate. Although some wake-up receivers may exceed SoMix in sensitivity, it is notable that SoMix, even when implemented with discrete components, achieves comparable sensitivity—indicating the potential for further improvement when realized as an integrated circuit. Moreover, SoMix may support complex modulation schemes such as FSK, CSS, and higher bitrates, as also supported by our experiments.

External local-oscillator architecture. SoMix is closely related to receiver architectures that leverage the non-linearity of Schottky diodes to receive complex modulated signals while maintaining a low-power consumption. A CED provides the carrier signal, which, due to the Schottky diode's non-linearity, is mixed with the received signal, resulting in the downconversion and generation of an IF signal. Ensworth et al. [44] designed a receiver compatible with the Bluetooth standard with a sensitivity of only -8 dBm with a carrier strength of 3 dBm, resulting in a range of a few meters. Penichet et al. designed an IEEE 802.15.4 receiver, but due to poor sensitivity, both the transmitter and the CED must be within tens of centimeters of the receiver [43]. Rostami et al. introduced a WiFi-compatible receiver that supports high data rate but has a limited range of a few tens of meters [29]. Li et al. achieved passive spread of the direct sequence spread spectrum (DSSS) signal by employing another channel to carry the synchronized spreading code, with an improved sensitivity of -45 dBm but a limited data rate [41]. Song et al. proposed the use of a pair of twin up chirps for CSS signal reception, achieving sensitivity and capability similar to LoRa. [40]. The low sensitivity and proximity requirements of CED restrict application scenarios for these receivers. In contrast, SoMix allows downconversion of signals as weak as -70 dBm, achieving a range exceeding 100 m, even when the CED located up to 100 m apart. Thus, SoMix significantly expands the range of possible application scenarios.

Commodity FSK receivers. We conducted a survey of commercial transceivers; among them, the Texas Instruments CC1101 and the Semtech SX1211 stand out in terms of sensitivity and power consumption. The SX1211 achieves a sensitivity of up to -107 dBm,

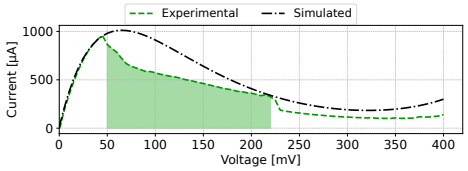

Figure 3: Tunnel diodes exhibit a region of negative differential resistance at low bias voltages and peak current levels, resulting in low-power consumption. We illustrate this characteristic for the specific tunnel diode in SoMix (GE 1N3712).

while the CC1101 reaches −112 dBm at a data rate of 1.2 kbps. However, both receivers draw several milliamperes of current, resulting in a power consumption of at least 10 mW at 3.3 V. These receivers consume at least an order of magnitude more power than SoMix, trading power efficiency for higher sensitivity.

Tunnel diode systems. A tunnel diode is a semiconductor device that exhibits negative resistance characteristics (NRC) in its current-voltage (I-V) curve, as shown in Figure 3. This unique property, where the current decreases as the bias voltage increases, arises from the quantum tunneling effect of tunnel diodes. The NRC makes tunnel diodes valuable for RF applications, such as reflection amplifiers [34, 52], low-power transmitters [11], and backscatter transmitters [34, 53]. Within this negative resistance region, small changes in the input voltage result in significant changes in current, allowing the sensitive detection of weak RF signals. This property enables tunnel diodes to efficiently rectify and detect low-level signals, as well as receive and injection-lock weak carrier signals.

Tunnel diodes have been used in communication systems for over a half century [54, 55]. Early designs explored their application in amplifiers [55], while others investigated their use in FM-broadcast transmitters [54]. However, their low output power and the challenges of working with a two-terminal device instead of a three-terminal transistor led to their decline. We build on these earlier efforts, recognizing that the limitations once considered now make tunnel diodes suitable for energy-constrained embedded systems.

There has been a growing interest in tunnel diode-based low-power communication mechanisms. Amato et al. designed a reflection amplifier capable of backscattering a 5.8 GHz signal over several kilometers [33, 52]. Varshney et al. demonstrated a reflection amplifier that enabled multi-floor communication using a 2-FSK modulation [34]. Dong et al. used a tunnel diode to relay the GPS signal, improving its propagation in indoor environments [37]. Thaddeus et al. explored the unstable nature of tunnel diode oscillator (TDO) for vital health sensing [38]. Mir et al. designed a low-power relay to transmit optical signals [35]. Building on these efforts, we designed a low-power oscillator. SoMix is most closely related to Judo, which demonstrated the self-oscillating mixing (SoM) property of TDOs to design a transmitter [11]. SoMix introduces, for the first time, the auto-dyning property of TDOs, enabling energy-efficient long-range reception. SoMix and Judo can work together to allow a transceiver design, which we discuss in Section 5.

3 Design

Embedded deployments employing a SoMix receiver consist of a CED, transmitters that send information, and devices equipped with the SoMix receivers. The process begins with the generation of a carrier signal by the TDO, which is stabilized through injection-locking using an carrier signal from the CED. The inherent non-linearity of

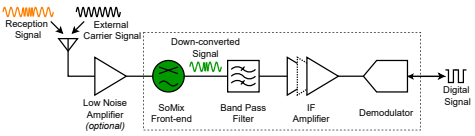

Figure 4: SoMix follows a pipelined architecture. The front-end first downconverts the received signal to an IF, passing through a bandpass filter to isolate the desired frequency components. The filtered signal is amplified using an IF amplifier and demodulated using a thresholding circuit, thus decoding transmitted information.

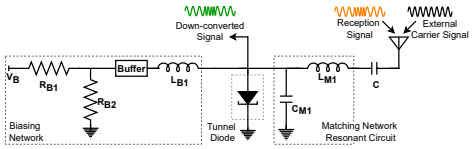

Figure 5: The SoMix front-end consists of a tunnel diode coupled with a resonant circuit, forming a TDO. This front-end exhibits an autodyning property, enabling the downconversion of incoming signals to IF signal under 100 μW power.

the tunnel diodes give rise to the autodyning property, allowing a single component to function as both the local oscillator and mixer, downconverting the incoming signal to an IF signal. Due to the sensitivity of the tunnel diode to weak radio signals, both the transmitter and the CED can be placed at significant distances from the device equipped with SoMix receiver. Figure 1 provides an overview of the embedded deployment, Figure 4 shows the receiver block diagram, and Figure 5 illustrates the SoMix front-end schematic.

3.1 Carrier Signal Generation and Stability

A local oscillator (LO) generates the carrier signal which is used to downconvert the received signals through mixers. While low-frequency oscillators used for baseband signal generation consume minimal power [9, 13, 14], high-frequency oscillators needed for the generation of carrier signals are power-intensive [8, 13]. SoMix uses TDO to generate the high-frequency carrier signal at lower-power.

Tunnel diode oscillators. When biased in the RNR and coupled to a resonant circuit, the tunnel diode generates oscillations [31, 34, 35, 38]. The TDO frequency can be tuned by adjusting the parameters of the resonant circuit. Due to the characteristics of tunnel diodes, carrier signals can be generated with a power consumption of the tens of μW [11, 34, 35]. Specifically, the TDO used in this work, based on the GE1N3712 tunnel diode [56], consumes less than 60 μW power consumption when biased in the RNR.

Carrier signal stability. Reliable communication requires stable carrier signals from the LO. The TDO trades off stability for low-power resulting in a high phase noise [34]. In addition, their frequency drifts due to environmental changes [11], nearby movements [38]. An analysis of the small-signal model of the reveals that its NRC depends on the shunting effect of the junction capacitance, which varies with frequency [31]. The effective negative resistance is:

$$R_{nr}{}' = \frac{R_{nr}}{(2\pi f C_d R_{nr})^2 + 1} \tag{1}$$

Here, $R_{nr}{}'$ represents the effective negative resistance, R_{nr} is the tunnel diode's intrinsic differential negative resistance, f is the frequency, and C_d is the junction capacitance. As frequency increases, the effective negative resistance decreases. The stability condition [57, 58] is expressed as:

$$\frac{L_T}{|R_{nr}{}'|C_d} < R_T < |R_{nr}{}'| \tag{2}$$

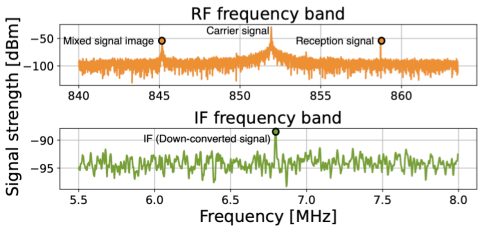

Figure 6: Due to the autodyning property of TDO, the received signal, the carrier signal, mixing products, and the IF signal are visible on the RF spectrum.

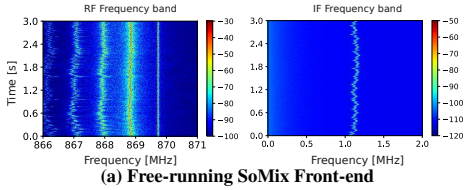

(a) Free-running SoMix Front-end

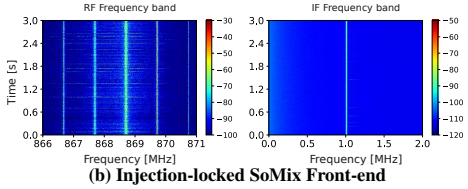

(b) Injection-locked SoMix Front-end

Figure 7: Injection-locking of the front-end improves TDO stability, and results in a stable IF signal even in the presence of motion in the vicinity of the front-end.

where L_T and R_T are the inductance and resistance of the lump circuit, including parasitic effects. This inequality becomes difficult to satisfy at higher frequencies, such as those used in embedded communication (sub-1 GHz, 2.4 GHz), posing challenges to stability.

Injection-locking to improve stability. To enhance the stability of the TDO, SoMix leverages the injection-locking phenomenon [11, 59]. Injection-locking occurs when two oscillators with similar resonant frequencies are coupled, causing them to synchronize and oscillate at the same frequency. In SoMix, when a CED generates a signal near the TDO's resonant frequency, the TDO locks onto this external carrier signal. This synchronization improves TDO's stability, enabling the SoMix front-end to generate a stable local carrier signal. The minimum signal strength required for injection-locking depends on the frequency difference between the TDO and the external carrier signal. This minimum is directly proportional to the injection current necessary to alter the frequency and is represented as follows.

$$I_i \approx 2QI_o \frac{|f_0 - f_c|}{f_0} \tag{3}$$

where I_i is the minimum injection current, I_o is the oscillator output current, Q is the quality factor, f_0 is the TDO's resonant frequency, and f_c is the external carrier signal frequency. A weak signal near the TDO's resonant frequency can achieve injection-locking [11]. Our observations show that the SoMix front-end can injection-lock with a signal of approximately -70 dBm, even when offset by a few hundred kilohertz from the TDO's resonant frequency.

3.2 Autodyne Mixing for Downconversion

The autodyne property of the TDO is the key to enable SoMix. This property allows the TDO to generate the carrier signal and downconvert the received signal in a single step, eliminating complex and energy-expensive mixer component.

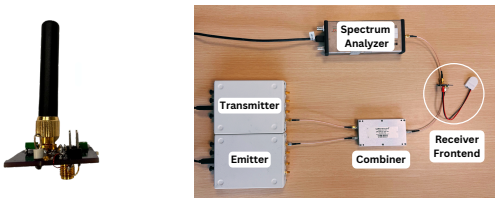

(a) Front-end **(b) Cabled Experimental Setup**

Figure 8: We conduct controlled experiments using a cabled setup to characterize the SoMix front-end, with a focus on evaluating its sensitivity and conversion-loss.

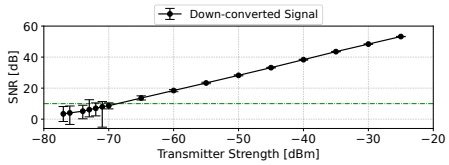

Figure 9: SoMix can receive and downconvert signals as weak as -70 dBm in our controlled experiments using a cabled setup. Additionally, the strength of the downconverted signal increases linearly with the strength of the incident signal, indicating that the conversion loss remains stable across input signal strengths.

Understanding non-linearity and role in downconversion. To understand how the non-linearity of tunnel diodes helps with downconversion, we can model the current that flows through the tunnel diode [60] and write it as follows.

$$I(V) = I_t + I_x + I_d = \frac{I_p V}{V_p} e^{\left(1-\frac{V}{V_p}\right)} + I_v e^{p(V-V_v)} + I_0 e^{\frac{qV}{kT}} \tag{4}$$

- I_t is the tunneling current, dominant for $V < V_v$,
- I_x is the excess current, significant near V_v,
- I_d is the diffusion current, dominant for $V > V_v$.

Here, I_p is peak current, V_p peak voltage, I_v valley current, V_v valley voltage, p a prefactor constant for the excess current, I_0 saturation current, q charge of an electron, and kT thermal voltage. While the model overestimates the current, it offers a method to analyze the mixing properties of the tunnel diode.

The first term $I_p \left(\frac{V}{V_p}\right) e^{1-\frac{V}{V_p}}$ models the negative resistance behavior. We can expand it using the power series expansion of $xe^{-x} = x - x^2 + \frac{x^3}{2!} - \frac{x^4}{3!} + \frac{x^5}{4!} + \ldots$ and use the approximation $xe^{-x} \approx x - x^2 + \frac{x^3}{2}$ as the high-order terms fall off with $\frac{1}{n!}$. Assuming $V_r = sin(2\pi f_r t)$ is the received RF signal and $V_c = sin(2\pi f_c t)$ corresponds to the carrier signal generated by the TDO circuit, the input signal applied to the diode is the sum of above two signals $V_r + V_c$. Then, the output voltage is proportional to the current flowing through the diode, which can be written as:

$$V_o \approx c \left((V_r + V_c) - \frac{1}{V_p}(V_r + V_c)^2 + \frac{1}{2V_p^2}(V_r + V_c)^3 \right) \tag{5}$$

where, c is a constant that accounts for the load impedance. The peak current (I_p) and the peak voltage (V_p) define the RNR. For the GE 1N3712 tunnel diode used in our design, I_p is 1 mA and V_p is 65 mV. In addition to the two original signals $V_r + V_c$, it includes the second and third-order terms, indicating that a group of harmonics and intermodulation products are generated. In second-order products, we get the harmonics at $2f_r$, $2f_c$, the high-frequency component at $f_r + f_c$, as well as the low-frequency component at $f_r - f_c$ that correspond to the downconverted IF signal f_d.

Illustrating downconversion. As shown in Figure 5, the TDO port serves two distinct functions. It receives the reception (target) signal,

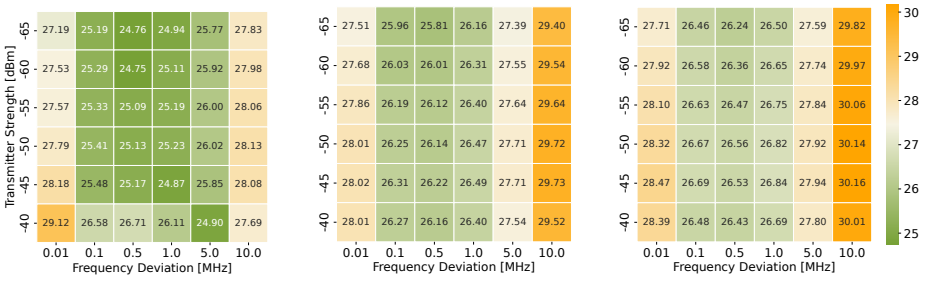

(a) IL Signal Strength= -40 dBm **(b) IL Signal Strength= -30 dBm** **(c) IL Signal Strength= -20 dBm**

Figure 10: The autodyne process in the TDO introduces conversion loss, resulting in a weaker downconverted signal compared to the received signal. This loss depends on several factors, including the strength of the injection-locking signal, the received signal, the frequency difference between the received signal and the IL signal.

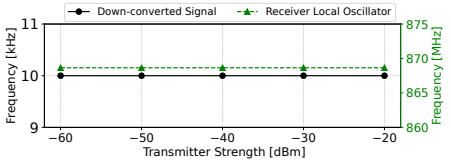

Figure 11: The SoMix front-end remains injection-locked and is not pulled toward the received signal, even as the received signal strength increases. This is evidenced by the stable frequency of the downconverted signal. Additionally, the strength of the downconverted signal scales linearly with the received signal strength.

and the same port is also used to extract the downconverted IF signal. We experimented to show the feasibility of the circuit to perform these operations. We generate the carrier signal using the TDO and then have a reception signal in the vicinity. Next, we capture the downconverted signal, which is the IF signal. Figure 6 shows that the downconverted IF signal frequency f_d is equal to the frequency difference between the reception signal and the carrier signal $f_r - f_c$. Furthermore, a mirror image of the signal appears at frequency $2f_c - f_r$ in the RF spectrum, corresponding to the intermodulation products of the third-order term in Equation 5.

Effect of frequency drift on downconversion. The SoMix can operate without injection-locking. However, this results in a broader oscillator peak because of higher phase noise and increased sensitivity to environmental factors and reception signal strength, which affects the stability of the TDO. In contrast, injection-locking provides stable and reliable downconversion. To evaluate these aspects, we experimented by programming USRP B200 [61] as the transmitter to generate a single-tone signal at a frequency 1 MHz offset from the TDO's resonant frequency. Figure 7 presents a waterfall plot that compares the SoMix free-running mode and the injection-locked mode using a spectrum analyzer [62]. In free-running mode, external motions near the TDO cause drifts in the frequency of the IF signal. Furthermore, we observed that increasing the transmitter strength causes the TDO's frequency to drift toward the reception signal, further affecting the IF signal frequency. This instability is effectively overcome by injection-locking, ensuring reliable reception.

Investigating receiver sensitivity. Receiver sensitivity refers to the minimum signal strength that can be reliably detected and processed to extract meaningful data. We conducted experiments using a wired setup to evaluate this, as shown in Figure 8 using two USRP B200 [61] for CED and transmitter, Signal Hound BB60C Spectrum Analyzer [62], Mini-Circuits ZN2PD2-63-S+ Power Splitter/Combiner [63] and the SoMix front-end. We varied the output power of the transmitter and measured the strength of the downconverted signal using a spectrum analyzer. A 10 kHz IF bandwidth was used to estimate the noise floor and calculate the signal-to-noise ratio (SNR). Figure 9 shows that the SNR of the downconverted signal increases with higher transmitter signal strength. The SoMix front-end can receive signals as weak as −80 dBm. For simple modulation schemes such as OOK, an SNR of at least 10 dB is typically required to achieve a low bit error rate (BER). Using this threshold, our results suggest that SoMix can reliably receive signals down to −70 dBm. It is important to note that this sensitivity measurement reflects the performance of the front-end alone. Sensitivity can be further improved with appropriate pre and IF amplification.

Understanding conversion loss. Next, we investigate whether there are losses during the downconversion process. Specifically, our objective is to understand the relationship between the strength of the downconverted signal and the strength of the received signal. We expect some loss, as the TDO may not be efficient in autodyning - partly because of the power distributed among multiple frequency components - and additional resistive losses in circuit components may further contribute to the overall conversion loss.

The conversion loss in the SoMix front-end may depend on several parameters of the received signal, including its strength, frequency, and the power of the injection-locking signal. To evaluate how these factors affect conversion loss, we conducted experiments using a cabled setup, similar to the sensitivity experiments, as shown in Figure 8b. Two USRP SDRs were used, one as the transmitter and the other as the CED. Their signals were propagated through a cabled setup, combined using an RF combiner, and fed to the SoMix front-end. We calibrated the output power of the SDRs and accounted for the losses of the RF combiner using a calibrated SignalHound BB60C spectrum analyzer. We varied the signal strength and frequency, and measured the strength of the downconverted IF signal using the spectrum analyzer. Because radio signals attenuate over distance and tunnel diodes operate in a narrow low-voltage range, we used signal strengths ranging from -20 dBm down to the lowest sensitivity threshold identified earlier. These values ensured that the tunnel diode remained within its negative resistance region and prevented damage from excessive input power. Figure 10 shows that the conversion loss remains relatively stable, averaging between 25 and 30 dB. Despite these losses, the SoMix front-end remains highly receptive to very weak signals.

Understanding the impact of received signal strength. We investigate how variations in the strength of the received signal affect the downconversion process when the TDO is injected. This analysis is essential because changes in signal strength could potentially disrupt the injection-locking process, causing the TDO to be pulled toward

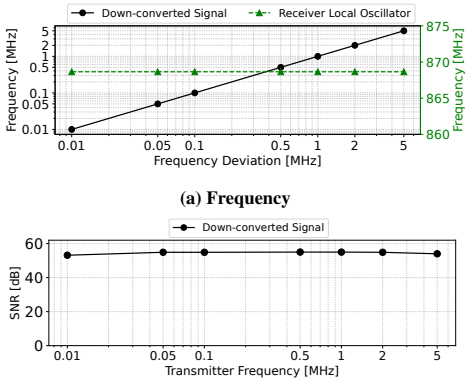

(a) Frequency

(b) Signal Strength

Figure 12: Altering the reception signal frequency, such as changing the communication channel, results in a corresponding shift in the IF signal frequency. Furthermore, the signal strength remains consistent throughout the experiment.

the received signal. We experimented with the cabled setup shown in Figure 8b, which was also used in previous experiments. The transmitted signal strength was varied from −60 dBm to −20 dBm in steps, while keeping the CED (injection-locking signal) strength constant at −20 dBm. As shown in Figure 11, we did not observe a significant change in the frequency of the IF signal or the LO, indicating that the front-end remained injection-locked to the carrier signal throughout. Furthermore, we observed a linear increase in the strength of the IF signal with received signal strength, also confirming stable conversion loss throughout this range.

Understanding the impact of received signal frequency. Finally, we examine how the frequency of the received signal affects the downconversion process. The transmitted signal remains within the same band with only minor adjustments, similar to what might occur in real-world scenarios when switching communication channels. This experiment was carried out using the same cabled setup shown in Figure 8b. We varied the transmitter frequency in steps to create offsets ranging from 10 kHz to 5 MHz relative to the frequency of the injection-locked TDO. We monitored both the frequency and the strength of the downconverted signal. As shown in Figure 12a, the frequency of the downconverted signal shifts accordingly with changes in the transmitter frequency. Furthermore, Figure 12b shows that the strength of the downconverted signal remains stable.

3.3 Enhancing IF Signal Strength

After the downconversion process, the resulting IF signal is weakened due to conversion losses. To extract meaningful information, especially in scenarios involving weak received signals, such as long-range communication, we incorporate an optional IF amplification stage. This stage enhances the sensitivity and facilitates digitization of the IF signal. Our design takes advantage of the fact that amplifiers operating at RF frequencies typically consume significantly more power than those operating at lower IF frequencies. This is mainly due to the higher gain-bandwidth product requirements and the complexity of managing impedance mismatches. In contrast, sub-MHz amplifiers can achieve high gain at µW-level power consumption, making them well-suited for low-power IF amplification.

When designing IF amplifiers, there is an inherent trade-off between gain and bandwidth. As the target frequency and bandwidth increase, the achievable gain decreases due to the fixed gain-bandwidth

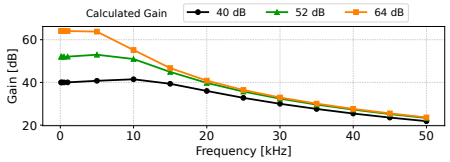

(a) Frequency Response of OPA330 op-amp

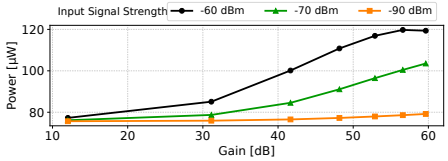

(b) Power Consumption

Figure 13: SoMix includes an optional IF amplification to support the reception of weak signals, balancing trade-offs among gain, bandwidth, and power.

product of the op-amp. Lower-frequency IF signals support higher gain with minimal power consumption, but limit the available bandwidth, and vice versa. To investigate this trade-off, we performed a SPICE simulation using a two-stage amplifier based on the Texas Instruments OPA330 [64], a micropower precision op-amp with a gain-bandwidth product of 350 kHz. Figure 13a shows how the available bandwidth decreases as the gain increases from 40 to 64 dB. Figure 13b further illustrates that power consumption increases with gain, underscoring the importance of careful design choices. Based on this analysis, we select an appropriate IF frequency and gain to strike a balance between performance and power efficiency. Our implementation uses a two-stage amplifier design, as shown in Figure 14, with each stage providing a small-signal voltage gain of 29 dB, resulting in a total gain of 58 dB. We also include a band-pass filter before amplification to isolate the desired IF signal and suppress harmonics, intermodulation products, and noise.

3.4 Digitizing Intermediate Frequency Signal

The final step in SoMix, as shown in Figure 14, involves digitizing the IF signal. We explored several options at this stage. We considered integrating low-power ADCs such as the ADS7042, which has been used in systems such as MIXIQ [29]. However, this method still consumes hundreds of µW and imposes significant processing overhead. To reduce power consumption, we adopted a comparator-based approach to digitizing the IF signal [8, 65]. In this approach, the amplified signal is fed into a comparator accompanied by a thresholding circuit implemented using passive RC filters. These filters track the long-term average of the signal, enabling the comparator to differentiate between high and low states by comparing the instantaneous signal value against this slowly changing reference.

We adapted the thresholding circuit to demodulate 2-FSK signals. For this, we used two frequencies, f_1 = 10 kHz and f_2 = 20 kHz, and configured the passband filter before amplification to allow f_1 while attenuating f_2. After amplification, the resulting signal resembles an ASK-modulated waveform, as illustrated in Figure 15, which can be digitized through the comparator. The frequency response is shown in Figure 13a. Although the voltage-level differences diminish with weaker signals, they remain distinguishable for the comparator to digitize reliably. We implemented this design using the nanopower TS881 comparator [66] and a 1N5819 diode [67]-based rectifier.

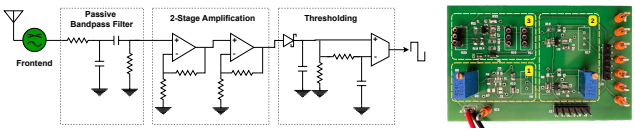

(a) Receiver Pipeline (b) PCB Prototype

Figure 14: The front-end performs the downconversion to the IF domain. The rest of the pipeline involves (1) extracting the baseband signal and filtering out the unwanted signals, (2) followed by 2-stage amplification and (3) finally demodulation.

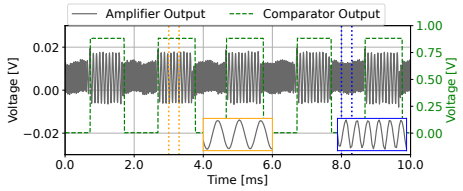

Figure 15: SoMix downconverts and transforms a 2-FSK signal into a signal that resembles an ASK signal and then is digitized using the comparator.

3.5 Putting Everything Together

SoMix operates as follows: An external carrier signal injection-locks the TDO, stabilizing it to generate a LO while simultaneously downconverting the incoming received signal. The resulting IF signal is filtered and amplified using a two-stage amplifier. The amplified signal is then digitized using a comparator-based design. The digitized signal is finally processed by the host microcontroller.

Illustrating frequency shift keying. We conduct experiments to evaluate the ability of the SoMix front-end to down-convert and receive 2-FSK transmissions. A USRP SDR is configured to transmit 2-FSK modulated signals and is placed 1 m from the SoMix front-end. A second USRP SDR, placed 2 m away, serves as the injection-lock CED. RF and IF signals received by the SoMix front-end are recorded using a spectrum analyzer, and the results are shown as waterfall graphs in Figure 16. Distinct modulation patterns are visible in the RF spectrum and the corresponding IF spectrum.

Power consumption. The SoMix front-end can be divided into three main components: the TDO circuit, the optional IF amplification and digitization stage, and the biasing circuit used to maintain the tunnel diode within its negative resistance region. The TDO circuit consumes less than 60 µW when powered by an external supply using the 1N3712 tunnel diode. For other tunnel diode variants, we conservatively estimate the power consumption of the front-end to remain under 100 µW. As implemented for the bitrates and bandwidths in this work, the IF amplification and digitization stage adds approximately 150 µW. The most power-consuming component is the biasing circuit, which brings the higher supply voltage down to the low voltage required to bias the tunnel diode in its negative resistance region. Specifically, we use a low-power DC-DC step-down converter to reduce a typical supply voltage (e.g., 3.3 V) to around 0.5 V. This reduced voltage is then regulated using a transistor and resistor network to bias the tunnel diode appropriately. This biasing circuit consumes approximately 250 µW.

3.6 Carrier Emitter Device

The CED generates a carrier signal, which can be easily generated using commodity transceivers found in everyday devices that support BLE [20] or other standards [14]. The power consumption is comparable to that of a typical radio transceiver, ranging from a few

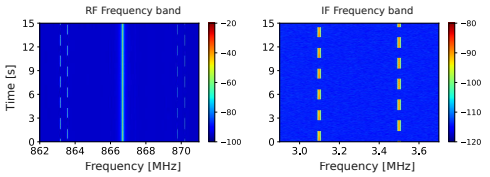

Figure 16: SoMix downconverts signals encoded with 2-FSK modulation visible through distinct patterns in the waterfall plot.

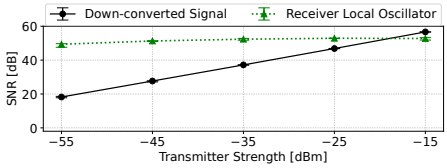

Figure 17: SoMix can be injection-locked to an unsuppressed carrier from the transmitter, which avoids the need for a dedicated carrier emitter device.

to hundreds of milliwatts, depending on the strength of the generated carrier signal. Since the SoMix can injection-lock to a weak carrier signal, the CED does not need to transmit at high power, allowing extended operation even when powered by a battery.

Asymmetric power. The CED consumes significantly more power than the SoMix, a common trait of low-power communication mechanisms, such as backscatter. However, in typical deployments, embedded devices transmit data to externally powered edge devices, making this power asymmetry practical in real-world scenarios.

Configuring frequency. A natural question is how the CED determines the frequency of the carrier signal and how often it must synchronize. The carrier signal should match the resonant frequency of TDO, although minor deviations are tolerable, as a strong carrier can pull the oscillator toward it. Since communication occurs on predefined channels set by standards, the receiver can operate on these channels and the CED can generate a signal accordingly. Once injection-locking is achieved, the frequency remains stable as long as no major obstructions disrupt the relative signal strength between the external carrier and the TDO, thereby avoiding the need for frequent reconfiguration of the carrier signal's frequency.

Eliminating CED. One approach to eliminate the need for a CED is to embed an unsuppressed carrier within the transmitted signal. This embedded carrier signal can be used for injection-locking, while the frequency-shifted portion of the signal carries the data for downconversion. By "unsuppressed carrier", we refer to transmissions in which the carrier signal is intentionally retained and transmitted along with the modulated data. In conventional AM with double sideband, for example, the carrier is transmitted along both sidebands. Similarly, unbalanced mixers allow the carrier to pass through, producing outputs that contain both the carrier and the modulated signals. This design is commonly seen in backscatter systems and in architectures such as Judo [11], which uses FSK while still radiating the original carrier. This stands in contrast to designs that suppress the carrier, such as double-sideband suppressed carrier systems that employ balanced mixers. We evaluated this approach by configuring the USRP transmitter to send an AM signal with a double-sideband, together with the carrier signal. The transmitter was connected to the front-end of SoMix by cable, and its carrier frequency was matched to the resonant frequency of SoMix, allowing stable injection-locking and down-conversion of the sidebands. As shown in Figure 17, the receiver maintains a stable local oscillator

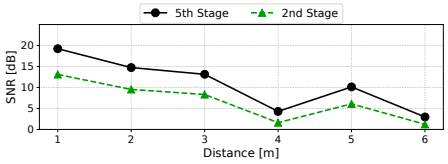

Figure 18: The physical limitations of Schottky diodes limit the sensitivity, and consequently, the range of the envelope detector to very short distances.

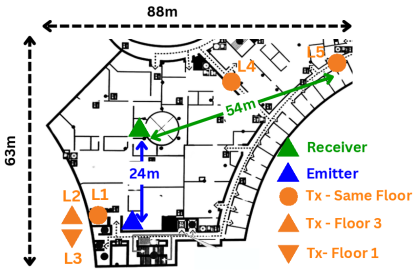

(a) Layout

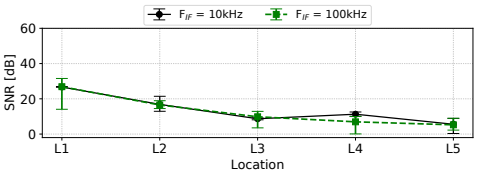

(b) SNR of Received Signal

Figure 19: The SoMix successfully downconverts signals even in complex NLoS environments involving multipath effects, maintaining an SNR greater than 5 dB.

frequency across varying transmitter signal strengths, demonstrating operation without a dedicated CED.

4 Evaluation

We evaluated SoMix under a variety of conditions. The key highlights of the results presented in this section are as follows.

- SoMix sensitivity of −70 dBm enables long-range reception in diverse environments achieving over 100 m range in LoS scenarios and up to 54 m in multipath-rich NLoS settings.
- SoMix supports bitrates of up to 10 kbps while operating with a front-end power consumption of less than 100 µW.

Setup. We used a USRP B200 SDR [61] to generate signals in a controlled manner. The SDRs were calibrated using a SignalHound BB60C spectrum analyzer [62], whose calibration we independently confirmed. The SDRs were used to generate both the carrier signal and the signal intended for reception by SoMix. A spectrum analyzer was used to observe various signals during the experiments, including the downconverted signal. The SDR, receiver, and transmitter were equipped with VERT900 antennas [68], which offer a typical antenna gain of 3 dBi. For wired experiments, we used a Mini-Circuits combiner. To increase the strength of radio signals for injection-locking and transmission, we employed a power amplifier rated for a maximum output of 30 dBm—the highest transmit power allowed by FCC regulations in unlicensed spectrum bands. This setup served as the experimental baseline configuration unless otherwise noted. Some experiments also incorporated an Analog Discovery 3 [69] and a digital oscilloscope to analyze baseband and IF signals. We conducted experiments in university lab environments for NLOS scenarios and in open areas for selected LOS experiments.

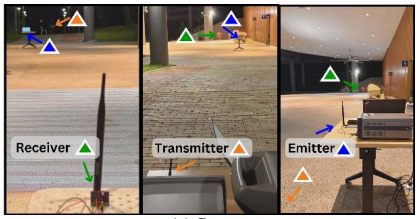

(a) Setup

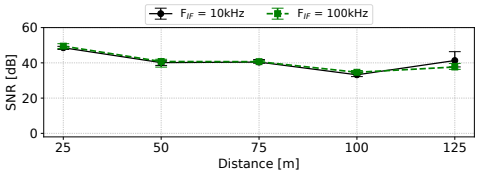

(b) SNR of Received Signal

Figure 20: SoMix receives transmissions with an SNR above 40 dB even with the transmitter at a distance of 125 m in a LoS complex propagation environment.

4.1 Downconversion and Communication Range

Benchmarking envelope detector. We design an envelope detector using HSMS286C Schottky diodes [36], arranged in multiple stages to achieve voltage doubling. Such designs are used on platforms such as WISP [50, 70, 71], Moo [72], and Ambient Backscatter tags [8]. We tune the envelope detector to operate in the sub-GHz band. For testing, we configured the USRP SDR to generate a carrier signal at the maximum supported power and monitor the received signal using a digital oscilloscope. Figure 18 shows the results that it achieves a range of only a few meters under LoS conditions before the signal drops near the noise floor. This result is consistent with previous systems that reported limited ranges using envelope detectors. The short range is primarily due to the inherent sensitivity limitations of Schottky diodes. These results help to establish a baseline.

SoMix in a NLoS environment. We evaluated the ability of the SoMix front-end to downconvert a received signal to an IF signal in a challenging indoor NLoS environment, representative of many real-world indoor deployments. In this experiment, we used a USRP B200 SDR as both the CED and the transmitter. Since the USRP supports a maximum output power of 16 dBm, we used an external power amplifier to increase the signal strength to 30 dBm, which is the maximum allowed under the FCC regulations [73]. We verified this output power using a calibrated spectrum analyzer. The transmitter was configured to generate signals at frequency offsets of 10 kHz and 100 kHz from the resonant frequency of TDO. These frequency separations between the injection-locking signal and the reception signal help prevent self-interference. The SoMix was connected to a spectrum analyzer to observe the downconverted IF signal and systematically measure the signal-to-noise ratio (SNR).

As shown in Figure 19a, we placed the SoMix receiver and CED at fixed locations, while changing the position of the transmitter across five different NLoS locations (L1 to L5). The locations L1, L2, and L3 are vertically aligned in the same section of the building: L1 on the same floor as the receiver, L2 on the top floor, and L3 on the bottom floor. The environment includes multiple walls, furniture, and other obstructions, creating a challenging propagation environment.

We present the results of the experiment in Figure 19b. The SoMix successfully downconverts signals across multiple locations, with the transmitter and receiver separated by distances of up to 54 m.

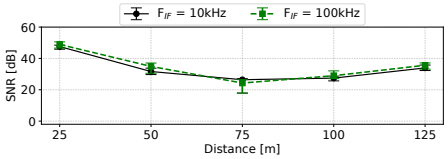

Figure 21: An unsuppressed carrier transmitted with the reception signal allows SoMix to avoid the CED. The range remains high.

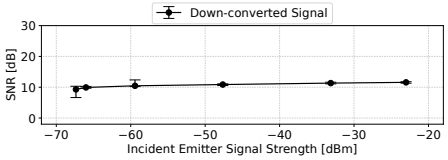

Figure 22: Varying the injection-locking signal strength does not affect the SNR of the downconverted signal, even when the signal strength is as low as -70 dBm. This ability to lock onto a weak carrier offers deployment flexibility for CED.

For all measurements, we maintained a minimum SNR threshold of approximately 5 dB to ensure reliable reception. Furthermore, we observed that varying the frequency deviation between the transmitted signal and the injection-locking signal (10 kHz and 100 kHz) did not have a significant impact on downconversion performance. These experiments were conducted in a university office setting, where considerable real-world interference from co-located devices, including lighting systems, HVAC units, and computing equipment, as well as concurrent wireless experiments operating in the same frequency band, was present. The receiver operates well consistently on multiple floors, demonstrating the feasibility of using SoMix for communication in complex indoor environments.

SoMix in a LoS environment. We evaluate the downconversion performance of SoMix in an LoS environment using a setup similar to the previous experiment to maintain consistency. The location of the experiment is the basement of a university building that opens to a road, as shown in Figure 20a. This environment introduces variations due to multipath effects caused by reflections from walls, ceilings, and nearby urban structures. For controlled evaluation, the CED is placed 25 m from the receiver and generates a carrier signal for injection-locking. This ensures consistency with other experiments in this work. However, in the LoS setup, the CED can be positioned more than 100 m away from the receiver if required.

The results, shown in Figure 20b, demonstrate that SoMix can successfully receive and downconvert signals from transmitters located over 125 m away. Even at this distance, the SNR remains well above 40 dB, sufficient to support complex modulation schemes, and suggests the potential for an even greater range. As in the previous experiment, the frequency deviation between the transmitted signal and the injection-locking signal (10 kHz vs. 100 kHz) does not significantly impact downconversion performance. It is important to note that these results were achieved using the front-end alone, without LNA-based amplification. SoMix already outperforms state-of-the-art receivers by a wide margin, and the results suggest that the range could be extended even further if required.

4.2 Easing CED Deployment

Eliminating CED. Incorporating an unsuppressed carrier signal into transmissions eliminates the need for a CED. The TDO locks onto the unsuppressed carrier, providing stability while simultaneously downconverting the signal, as described in Section 3.2. We

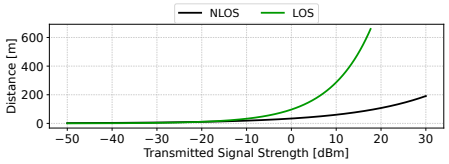

Figure 23: An analytical evaluation of SoMix 's range suggests it can achieve communication distances of several hundred meters, even in complex environments.

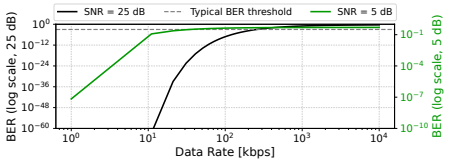

Figure 24: Estimating the upper bound on bitrate through theoretical analysis—based on the achieved SNR values and a BER threshold of 10^{-3}—suggests that data rates exceeding 10 kbps are achievable even in complex environments.

used a setup similar to the previous experiment (Section 4.1) to evaluate the range. The transmitter was configured to include an unsuppressed carrier, with the message signal offset by 10 kHz and 100 kHz to avoid self-interference, consistent with previous experiments. Figure 21 presents the results, which match those of the previous experiment involving a CED. We successfully communicated at distances up to 125 m, with an SNR of 40 dB. These findings suggest that even longer communication ranges are possible, if needed.

Weak injection-locking signal. SoMix can achieve injection locking with a weak carrier signal, allowing greater separation between the CED and SoMix and providing flexibility of deployment. We fixed the distance between the SoMix receiver and the USRP transmitter at 10 m in an indoor environment, with the transmitted signal strength set at -20 dBm, representative of weak, but realistic, indoor signal levels. A second USRP served as the CED, and its distance from the receiver was varied in an NLoS environment to change the strength of the incident injection-locking signal. A spectrum analyzer was used to observe both the injection-locking signal and the corresponding downconverted signal. The results, shown in Figure 22, indicate that the SNR of the downconverted signal remains stable even when the strength of the injection locking signal drops to approximately -70 dBm. This confirms that weak carrier signals are sufficient to stabilize TDO in SoMix, allowing reception even when the CED is located a significant distance from the receiver.

4.3 Bit Rate, Bit Error Rate, and Link Budget

SoMix link budget. We analyze the SoMix receiver's communication capability using the ITU-R P.1411 propagation model [74], which is designed for outdoor short-range communication between 300 MHz and 100 GHz. Unlike Friis' model, it accounts for terrain, buildings, and obstructions, making it suitable for urban high-rise environments characterized by urban canyons, reflections, and Doppler shifts, with minimal rooftop propagation. Figure 23 shows the estimated maximum ranges at 868 MHz with 30 dBm transmission power (per FCC limits). Assuming a sensitivity of −70 dBm, the receiver achieves ranges of 191 m in NLoS and over 660 m in LoS conditions (model valid only up to 660 m). Indeed, our experimental results, presented in Section 4.1, support the high link budget.

SoMix bitrate and bit error rate. We begin by theoretically estimating the maximum achievable bitrate using established models [75].

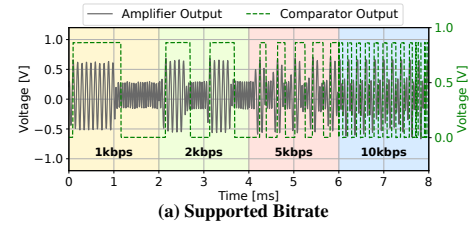

(a) Supported Bitrate

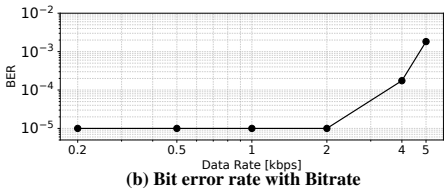

(b) Bit error rate with Bitrate

Figure 25: An end-to-end evaluation of SoMix under varying bitrates suggests that the bit error rate increases at higher bitrates due to trade-offs made to reduce power consumption in the IF amplification stage and digitization mechanism.

This estimate is based on the SNR values of 25 dB and 5 dB, which, as demonstrated in our experiments, can be achieved at considerable communication distances, for example in NLoS environment at locations L1 (25 m) and L5 (54 m). Figure 24 presents the estimated maximum bitrate assuming a BER threshold of 10^{-3} for 2-FSK modulation. The results show that even under challenging NLoS conditions, SoMix could support data rates exceeding 10 kbps.

Next, we empirically evaluate the bitrate supported by SoMix by examining its ability to demodulate and digitize received signals, representing an end-to-end evaluation of the receiver. The experiment was carried out in an indoor university office using two USRP SDRs, one acting as the transmitter and the other as the CED, placed 10 m from the SoMix receiver. The transmitter was configured to send a 2-FSK signal with frequency deviations of $f_1 = 10$ kHz and $f_2 = 20$ kHz from the resonant frequency of the TDO. This small frequency deviation presents a challenging scenario due to the increased complexity in filter design and limited bandwidth, which constrains the achievable bitrate. We varied the bitrate from 0.2 kbps to 5 kbps. Each transmission included a 1-byte preamble for synchronization followed by a 24-byte payload. We transmitted each packet 150 times, thus totaling 30,000 sent bits.

Figure 25 shows the results of the experiment. The comparator successfully digitized the bit transitions at all tested bitrates. BER remained low even at the highest rate tested of 5 kbps. In particular, this BER was measured without error correction or additional redundancy, which could further improve performance. Moreover, higher bitrates are feasible by increasing the frequency deviation and adapting the filter design within SoMix accordingly.

Finally, we evaluate the performance of SoMix at varying distances between the transmitter and the receiver. This experiment was carried out in an LoS environment, with the CED placed 25 m from the receiver, consistent with previous experiment setups. We varied the transmitter distance from the receiver in increments of 10 m and configured it to transmit at a bitrate of 1 kbps. Figure 26 presents the results. The BER remains reasonable even at larger distances between the transmitter and receiver. However, it is higher than what is observed with commodity transceivers. The higher BER can be attributed to several factors: the use of a comparator and thresholding circuit that effectively acts as a 1-bit ADC, which, while energy efficient, struggles to distinguish between signal levels in the presence of ambient noise; operation in an uncontrolled frequency band with potential interference; and limited IF gain to reduce power consumption, which compromises robustness during digitization.

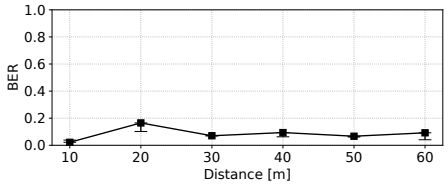

Figure 26: BER of the SoMix with varying distances up to 60 m in a LoS setup.

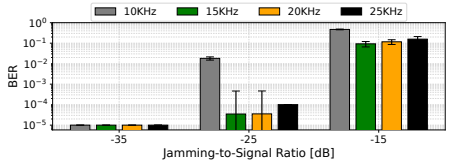

Figure 27: SoMix receiver performs well under moderate interference conditions. Under strong interference, the receiver's performance deteriorates.

4.4 Performance under External Interference

We evaluate the impact of interference on SoMix. Given the design trade-offs made to minimize power consumption, we anticipate that external interference could affect link reliability. To ensure consistency, we used a setup similar to that of previous experiments, with the addition of a USRP SDR configured to generate a controlled jamming signal at varying signal strengths. The transmitter, CED, and interferer are placed 10 m from the receiver, representing common deployment scenarios such as smart homes. We use the jamming-to-signal ratio (JSR) in dB as the evaluation metric, indicating the difference in signal strength between the jamming and transmitter signals. The transmitter operates with 2-FSK modulation at a bitrate of 2 kbps, using frequency deviations of $f_1 = 10$ kHz and $f_2 = 20$ kHz. Figure 27 shows the results of the experiment. As expected, the BER remains low when the JSR is below -25 dB. However, as the jamming signal strength approaches that of the transmitter, the BER increases significantly, indicating that the receiver struggles to decode reliably in the presence of strong interference.

5 Discussion and Conclusion

We present SoMix, a low-power receiver architecture that enables long-range reception. Its contribution lies in demonstrating the autodyning property of TDO. Our experiments show that SoMix can downconvert signals as weak as -70 dBm, achieving reception at distances exceeding 100 m in LOS and 54 m in NLOS environments.

Two-way communication. Low-power transmission is achievable using the backscatter mechanism [9, 12, 14, 51] and designs based on TDO [11, 34]. By integrating SoMix with them, it becomes possible to design a transceiver capable of two-way communication. We experimented to evaluate the feasibility of combining Judo with SoMix. The TDO was configured to operate at 868 MHz and was injection-locked using a carrier signal from a CED placed 5 m away. A separate transmitter, also located 5 m from SoMix, transmitted a signal at 869.3 MHz. Simultaneously, the TDO was modulated for transmission with a 500 kHz baseband signal. Figure 28 presents the resulting spectrum, showing the received signal, the mixed transmission signal due to the SoM property of the TDO, the injection-locked signal, and additional harmonics. We observe that the downconverted

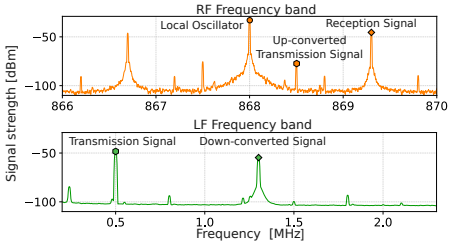

Figure 28: We observe both the transmission signal, enabled by the SoM property of the TDO, and the downconverted IF signal resulting from its autodyning property. SoMix can allow the design of a transceiver enabling two-way communication.

IF signal (for reception) and the upconverted transmission signal appear distinctly. Since the TDO front-end is reused for both transmitting and receiving, we expect the total power of the transceiver to remain comparable to that of the standalone SoMix and Judo.

Commodity standards. SoMix may enable the design of receivers that support commodity standards based on complex modulation, such as Wi-Fi and LTE-NB (which use OFDM), and LoRa (which uses CSS). Its combination of high-sensitivity, low-power consumption, and ability to downconvert weak signals makes it well-suited for deployment in challenging scenarios where state-of-the-art low-power receivers typically fall short. We provide early evidence supporting the viability of SoMix for downconverting chirp-modulated transmissions, which are used in standards such as LoRa. In a controlled setup, an SDR transmitter generates chirps over a 500 kHz bandwidth at four different rates, ranging from 0.5 to 4 chirps/second. The transmitter is connected to the TDO receiver through an RF cable, with the transmitted signal strength set to −57 dBm. Figure 29a shows the results, where the chirps are clearly visible in both the RF and the IF bands. We also evaluated the system under realistic NLOS conditions: the SoMix receiver was placed in one room, while the transmitter was placed 18 m away in another room, separated by multiple walls. The transmitter emitted chirps at a rate of 1 chirp/second with a signal strength of 16 dBm. As shown in Figure 29b, chirps remain visible in both the RF and the IF bands. Despite the complex indoor environment and weak received signal, SoMix downconverts the chirp-modulated signal, demonstrating its potential to support the design of receivers compatible with the LoRa standard.

Tag-to-tag networks. There has been interest in networks in which both the transmitter and receiver are passive devices, a vision introduced by ambient backscatter [8]. However, even a decade after its demonstration, such networks have yet to be deployed in the real world. We argue that a key reason for this is the reliance on classical envelope detectors, which suffer from a limited range, typically only a few tens of centimeters. In contrast, SoMix, with its ability to receive weak signals over significantly longer distances, may help overcome these limitations. To evaluate this, we generate a 16 dBm carrier signal to injection-lock the SoMix. The CED and the SoMix receiver are placed 5 m apart. We program the backscatter tag to alternately reflect and absorb signals at a frequency of 5 MHz and observe the received signal at SoMix. The same carrier signal is used for both injection-locking and backscattering. As shown in Figure 30, SoMix successfully downconverts the backscattered signal while maintaining sufficient signal strength. The downconverted signal exceeds the SoMix sensitivity threshold, suggesting that with a sufficiently strong carrier, SoMix could enable tag-to-tag networks with ranges extending to tens of meters.

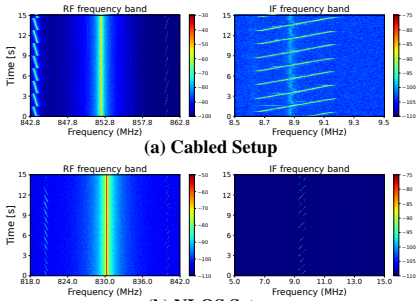

Figure 29: SoMix supports the downconversion of signals with complex modulation.

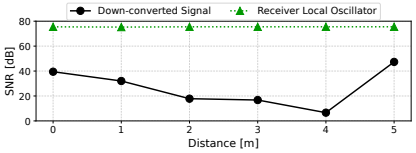

Figure 30: The SoMix front-end's high sensitivity allows it to receive weak backscattered signals. This may pave the way for tag-to-tag networking at large distances.

Beyond reception. Envelope detectors have been used for applications such as localization [76] and gesture recognition [77]. However, their reliance on amplitude-only extraction limits their capabilities. By allowing for the extraction of phase, frequency and amplitude, the SoMix front-end offers the potential to enhance these scenarios.

Tunnel diodes. They are commercially obsolete. Their decline, historically attributed to limited power output and the challenges in achieving scalability with silicon-based manufacturing processes [31]. At their core, tunnel diodes rely on a heavily doped semiconductor junction, employing materials such as gallium arsenide (GaAs) or germanium (Ge). In contrast, most contemporary integrated circuits rely predominantly on silicon-based CMOS processes optimized for scalability and high-yield manufacturing. This fundamental material and fabrication mismatch presents a technical challenge: the integration of non-silicon-based tunnel diodes within silicon CMOS fabrication workflows to achieve low-power, integrated system-on-chip designs. Some advanced heterogeneous integration techniques, such as hybrid integration, wafer bonding, or monolithic integration, using compound semiconductor epitaxial growth on silicon substrates, may help us integrate tunnel diodes. Recent efforts [11, 33–35, 37, 52, 78, 79] demonstrate the potential of tunnel diodes in low-power communication circuits, which can motivate the integration of tunnel diodes into modern processes.

Acknowledgments

The authors thank the reviewers and the shepherd for their feedback. The authors acknowledge Dr. Amalinda Gamage, Dr. Manoj Gulati, Spanddhana Sara and Dhairya Shah for their support. This work was supported by a Tier-1 grant from the Ministry of Education (A-8001661-00-00), a startup grant from ODPT (A-8000277-00-00), an unrestricted gift from Google through their Google Research Scholar Program (A-8002307-00-00-00)— hosted at the National University of Singapore, and Okawa Foundation Research Grant awarded to Prabal Dutta at the University of California, Berkeley.

References

[1] Vamsi Talla, Bryce Kellogg, Shyamnath Gollakota, and Joshua R. Smith. Battery-free cellphone. *Proc. ACM Interact. Mob. Wearable Ubiquitous Technol.*, 1(2), June 2017.

[2] Saman Naderiparizi, Mehrdad Hessar, Vamsi Talla, Shyamnath Gollakota, and Joshua R. Smith. Towards battery-free hd video streaming. In *Proceedings of the 15th USENIX Conference on Networked Systems Design and Implementation*, NSDI'18, page 233–247, USA, 2018. USENIX Association.

[3] Pengyu Zhang, Pan Hu, Vijay Pasikanti, and Deepak Ganesan. Ekhonet: High speed ultra low-power backscatter for next generation sensors. In *Proceedings of the 20th Annual International Conference on Mobile Computing and Networking*, MobiCom '14, page 557–568, New York, NY, USA, 2014. Association for Computing Machinery.

[4] Xin Na, Xiuzhen Guo, Zihao Yu, Jia Zhang, Yuan He, and Yunhao Liu. Leggiero: Analog wifi backscatter with payload transparency. In *Proceedings of the 21st Annual International Conference on Mobile Systems, Applications and Services*, MobiSys '23, page 436–449, New York, NY, USA, 2023. Association for Computing Machinery.

[5] Ambuj Varshney, Andreas Soleiman, Luca Mottola, and Thiemo Voigt. Battery-free visible light sensing. In *Proceedings of the 4th ACM Workshop on Visible Light Communication Systems*, VLCS '17, page 3–8, New York, NY, USA, 2017. Association for Computing Machinery.

[6] Robert Szewczyk, Alan Mainwaring, Joseph Polastre, John Anderson, and David Culler. An analysis of a large scale habitat monitoring application. In *Proceedings of the 2nd International Conference on Embedded Networked Sensor Systems*, SenSys '04, page 214–226, New York, NY, USA, 2004. Association for Computing Machinery.

[7] Shuai Tong, Jiliang Wang, Jing Yang, Yunhao Liu, and Jun Zhang. Citywide lora network deployment and operation: Measurements, analysis, and implications. In *Proceedings of the 21st ACM Conference on Embedded Networked Sensor Systems*, SenSys '23, page 362–375, New York, NY, USA, 2024. Association for Computing Machinery.

[8] Vincent Liu, Aaron Parks, Vamsi Talla, Shyamnath Gollakota, David Wetherall, and Joshua R. Smith. Ambient backscatter: wireless communication out of thin air. In *Proceedings of the ACM SIGCOMM 2013 Conference on SIGCOMM*, SIGCOMM '13, page 39–50, New York, NY, USA, 2013. Association for Computing Machinery.

[9] Bryce Kellogg, Vamsi Talla, Joshua R. Smith, and Shyamnath Gollakot. Passive wi-fi: Bringing low power to wi-fi transmissions. *GetMobile: Mobile Comp. and Comm.*, 20(3):38–41, January 2017.

[10] Vamsi Talla, Mehrdad Hessar, Bryce Kellogg, Ali Najafi, Joshua R. Smith, and Shyamnath Gollakota. Lora backscatter: Enabling the vision of ubiquitous connectivity. *Proc. ACM Interact. Mob. Wearable Ubiquitous Technol.*, 1(3), September 2017.

[11] Ambuj Varshney, Wenqing Yan, and Prabal Dutta. Judo: addressing the energy asymmetry of wireless embedded systems through tunnel diode based wireless transmitters. In *Proceedings of the 20th Annual International Conference on Mobile Systems, Applications and Services*, MobiSys '22, page 273–286, New York, NY, USA, 2022. Association for Computing Machinery.

[12] Joshua F. Ensworth and Matthew S. Reynolds. Every smart phone is a backscatter reader: Modulated backscatter compatibility with bluetooth 4.0 low energy (ble) devices. In *2015 IEEE International Conference on RFID (RFID)*, pages 78–85, 2015.

[13] Pengyu Zhang, Mohammad Rostami, Pan Hu, and Deepak Ganesan. Enabling practical backscatter communication for on-body sensors. In *Proceedings of the 2016 ACM SIGCOMM Conference*, SIGCOMM '16, page 370–383, New York, NY, USA, 2016. Association for Computing Machinery.

[14] Ambuj Varshney, Oliver Harms, Carlos Pérez-Penichet, Christian Rohner, Frederik Hermans, and Thiemo Voigt. Lorea: A backscatter architecture that achieves a long communication range. In *Proceedings of the 15th ACM Conference on Embedded Network Sensor Systems*, SenSys '17, New York, NY, USA, 2017. Association for Computing Machinery.

[15] Tijs van Dam and Koen Langendoen. An adaptive energy-efficient mac protocol for wireless sensor networks. In *Proceedings of the 1st International Conference on Embedded Networked Sensor Systems*, SenSys '03, page 171–180, New York, NY, USA, 2003. Association for Computing Machinery.

[16] Wei Ye, J. Heidemann, and D. Estrin. An energy-efficient mac protocol for wireless sensor networks. In *Proceedings.Twenty-First Annual Joint Conference of the IEEE Computer and Communications Societies*, volume 3, pages 1567–1576 vol.3, 2002.

[17] Prabal Dutta, Stephen Dawson-Haggerty, Yin Chen, Chieh-Jan Mike Liang, and Andreas Terzis. A-mac: A versatile and efficient receiver-initiated link layer for low-power wireless. *ACM Trans. Sen. Netw.*, 8(4), September 2012.

[18] Michael Buettner, Gary V. Yee, Eric Anderson, and Richard Han. X-mac: a short preamble mac protocol for duty-cycled wireless sensor networks. In *Proceedings of the 4th International Conference on Embedded Networked Sensor Systems*, SenSys '06, page 307–320, New York, NY, USA, 2006. Association for Computing Machinery.

[19] Adam Dunkels. The contikimac radio duty cycling protocol, 2011.

[20] Vikram Iyer, Vamsi Talla, Bryce Kellogg, Shyamnath Gollakota, and Joshua Smith. Inter-technology backscatter: Towards internet connectivity for implanted devices. In *Proceedings of the 2016 ACM SIGCOMM Conference*, SIGCOMM '16, page 356–369, New York, NY, USA, 2016. Association for Computing Machinery.

[21] Jason Hill, Robert Szewczyk, Alec Woo, Seth Hollar, David Culler, and Kristofer Pister. System architecture directions for networked sensors. *SIGARCH Comput. Archit. News*, 28(5):93–104, November 2000.

[22] Romit Roy Choudhury. Earable computing: A new area to think about. In *Proceedings of the 22nd International Workshop on Mobile Computing Systems and Applications*, HotMobile '21, page 147–153, New York, NY, USA, 2021. Association for Computing Machinery.

[23] Kunjun Li, Manoj Gulati, Dhairya Shah, Steven Waskito, Shantanu Chakrabarty, and Ambuj Varshney. Pixelgen: Rethinking embedded cameras for mixed-reality. In *Proceedings of the 30th Annual International Conference on Mobile Computing and Networking*, ACM MobiCom '24, page 2128–2135, New York, NY, USA, 2024. Association for Computing Machinery.

[24] Jingyu Lee, Hyunsoo Kim, Minjae Kim, Byung-Gon Chun, and Youngki Lee. Maestro: The analysis-simulation integrated framework for mixed reality. In *Proceedings of the 22nd Annual International Conference on Mobile Systems, Applications and Services*, MOBISYS '24, page 99–112, New York, NY, USA, 2024. Association for Computing Machinery.

[25] Maximilian Speicher, Brian D. Hall, and Michael Nebeling. What is mixed reality? In *Proceedings of the 2019 CHI Conference on Human Factors in Computing Systems*, CHI '19, page 1–15, New York, NY, USA, 2019. Association for Computing Machinery.

[26] A.-J. Annema. Analog circuit performance and process scaling. *IEEE Transactions on Circuits and Systems II: Analog and Digital Signal Processing*, 46(6):711–725, 1999.

[27] A.-J. Annema, B. Nauta, R. van Langevelde, and H. Tuinhout. Analog circuits in ultra-deep-submicron cmos. *IEEE Journal of Solid-State Circuits*, 40(1):132–143, 2005.

[28] E.A. Vittoz. Low-power design: ways to approach the limits. In *Proceedings of IEEE International Solid-State Circuits Conference - ISSCC '94*, pages 14–18, 1994.

[29] Mohammad Rostami, Xingda Chen, Yuda Feng, Karthikeyan Sundaresan, and Deepak Ganesan. MIXIQ: re-thinking ultra-low power receiver design for next-generation on-body applications. In *Proceedings of the 27th Annual International Conference on Mobile Computing and Networking*, MobiCom '21, page 364–377, New York, NY, USA, 2021. Association for Computing Machinery.

[30] J. Ensworth et al. *Ultra-low-power Bluetooth Low Energy (BLE) compatible backscatter communication and energy harvesting for battery-free wearable devices*. PhD thesis, 2016.

[31] RCA Corporation. Semiconductor and Materials Division. *RCA Tunnel Diode Manual*. RCA technical manual. RCA, 1963.

[32] Francesco Amato. *Achieving hundreds-meter ranges in low powered RFID systems with quantum tunneling tags*. PhD thesis, GaTecH, 2017.

[33] Francesco Amato, Christopher W. Peterson, Brian P. Degnan, and Gregory D. Durgin. Tunneling rfid tags for long-range and low-power microwave applications. *IEEE Journal of Radio Frequency Identification*, 2(2):93–103, 2018.

[34] Ambuj Varshney, Andreas Soleiman, and Thiemo Voigt. Tunnelscatter: Low power communication for sensor tags using tunnel diodes. In *The 25th Annual International Conference on Mobile Computing and Networking*, MobiCom '19, New York, NY, USA, 2019. Association for Computing Machinery.

[35] Muhammad Sarmad Mir, Wenqing Yan, Prabal Dutta, Domenico Giustiniano, and Ambuj Varshney. Tunnellifi: Bringing lifi to commodity internet of things devices. In *Proceedings of the 24th International Workshop on Mobile Computing Systems and Applications*, HotMobile '23, page 1–7, New York, NY, USA, 2023. Association for Computing Machinery.

[36] Broadcom. Hsms-286c schottky diode. https://www.broadcom.com/products/optical-solutions/diodes/hsms-286c. Accessed: 2024-12-01.

[37] Huixin Dong, Yirong Xie, Xianan Zhang, Wei Wang, Xinyu Zhang, and Jianhua He. Gpsmirror: Expanding accurate gps positioning to shadowed and indoor regions with backscatter. 2023.

[38] Lim Chang Quan Thaddeus, C. Rajashekar Reddy, Yuvraj Singh Bhadauria, Dhairya Shah, Manoj Gulati, and Ambuj Varshney. Tunnelsense: Low-power, non-contact sensing using tunnel diodes. In *2024 IEEE International Conference on RFID (RFID)*, pages 154–159, 2024.

[39] B. Razavi. A study of injection locking and pulling in oscillators. *IEEE Journal of Solid-State Circuits*, 39(9):1415–1424, 2004.

[40] Yihang Song, Li Lu, Jiliang Wang, Chong Zhang, Hui Zheng, Shen Yang, Jinsong Han, and Jian Li. μMote: Enabling passive chirp de-spreading and uw-level long-range downlink for backscatter devices. In *20th USENIX Symposium on Networked Systems Design and Implementation (NSDI 23)*, pages 1751–1766, Boston, MA, April 2023. USENIX Association.

[41] Songfan Li, Hui Zheng, Chong Zhang, Yihang Song, Shen Yang, Minghua Chen, Li Lu, and Mo Li. Passive DSSS: Empowering the downlink communication

for backscatter systems. In *19th USENIX Symposium on Networked Systems Design and Implementation (NSDI 22)*, pages 913–928, Renton, WA, April 2022. USENIX Association.

[42] Xiuzhen Guo, Longfei Shangguan, Yuan He, Nan Jing, Jiacheng Zhang, Haotian Jiang, and Yunhao Liu. Saiyan: Design and implementation of a low-power demodulator for LoRa backscatter systems. In *19th USENIX Symposium on Networked Systems Design and Implementation (NSDI 22)*, pages 437–451, Renton, WA, April 2022. USENIX Association.

[43] Carlos Pérez-Penichet, Claro Noda, Ambuj Varshney, and Thiemo Voigt. Battery-free 802.15.4 receiver. In *2018 17th ACM/IEEE International Conference on Information Processing in Sensor Networks (IPSN)*, pages 164–175, 2018.

[44] Joshua F. Ensworth, Alexander T. Hoang, and Matthew S. Reynolds. A low power 2.4 ghz superheterodyne receiver architecture with external lo for wirelessly powered backscatter tags and sensors. In *2017 IEEE International Conference on RFID (RFID)*, pages 149–154, 2017.

[45] Heyu Ren, Liangjian Lyu, Binbin Chen, Wenjun Gong, Xing Wu, and C.-J. Richard Shi. A 225-uw interference-tolerant receiver with shared wireless lo and envelope-tracking mixer achieving -104-dbm sensitivity. *IEEE Journal of Solid-State Circuits*, 60(3):755–767, 2025.

[46] Erkan Alpman, Ahmad Khairi, Richard Dorrance, Minyoung Park, V. Srinivasa Somayazulu, Jeffrey R. Foerster, Ashoke Ravi, Jeyanandh Paramesh, and Stefano Pellerano. 802.11g/n compliant fully integrated wake-up receiver with -72 dbm sensitivity in 14-nm finfet cmos. *IEEE Journal of Solid-State Circuits*, 53(5):1411–1422, 2018.

[47] Jaeho Im, Hun-Seok Kim, and David D. Wentzloff. A 335uw -72dbm receiver for fsk back-channel embedded in 5.8ghz wi-fi ofdm packets. In *2017 IEEE Radio Frequency Integrated Circuits Symposium (RFIC)*, pages 176–179, 2017.

[48] Camilo Salazar, Andreia Cathelin, Andreas Kaiser, and Jan Rabaey. A 2.4 ghz interferer-resilient wake-up receiver using a dual-if multi-stage n-path architecture. *IEEE Journal of Solid-State Circuits*, 51(9):2091–2105, 2016.

[49] Xiongchuan Huang, Pieter Harpe, Guido Dolmans, Harmke de Groot, and John R. Long. A 780–950 mhz, 64–146 µw power-scalable synchronized-switching ook receiver for wireless event-driven applications. *IEEE Journal of Solid-State Circuits*, 49(5):1135–1147, 2014.

[50] S. Naderiparizi, A. N. Parks, Z. Kapetanovic, B. Ransford, and J. R. Smith. Wispcam: A battery-free rfid camera. In *IEEE RFID 2015*, 2015.

[51] Shih-Kai Kuo, Manideep Dunna, Dinesh Bharadia, and Patrick P. Mercier. A wifi and bluetooth low-energy backscatter combo chip with beam steering capabilities. *IEEE Open Journal of the Solid-State Circuits Society*, 3:239–248, 2023.

[52] Francesco Amato, Christopher W. Peterson, Muhammad B. Akbar, and Gregory D. Durgin. Long range and low powered rfid tags with tunnel diode. In *2015 IEEE International Conference on RFID Technology and Applications (RFID-TA)*, pages 182–187, 2015.

[53] Francesco Amato and Gregory D Durgin. Tunnel diodes for backscattering communications. In *2018 2nd URSI Atlantic Radio Science Meeting (AT-RASC)*, pages 1–3. IEEE, 2018.

[54] W. Ko, W. Thompson, and E. Yon. A tunnel-diode fm transmitter for medical research and laboratory telemetering. In *1962 IEEE International Solid-State Circuits Conference. Digest of Technical Papers*, volume V, pages 70–71, 1962.

[55] L. Armstrong. Tunnel diodes for low noise amplification. In *1961 International Electron Devices Meeting*, pages 62–62, 1961.

[56] General Electric. Tunnel Diode 1N3712.

[57] Sylvester P. Gentile. *Basic Theory and Application of Tunnel Diodes*. D Van Nostrand Company Inc, 1962.

[58] G. T. Munsterman. Tunnel-diode microwave amplifiers. *APL Technical Digest*, 1965.

[59] B. Razavi. A study of injection locking and pulling in oscillators. *IEEE Journal of Solid-State Circuits*, 39(9):1415–1424, Sep. 2004.

[60] S.M. Sze and Kwok K. Ng. *Physics of Semiconductor Devices*. John Wiley & Sons, Hoboken, NJ, 3rd edition, 2006.

[61] Ettus Research. B200/b210 software defined radio (sdr) spec sheet. https://www.ettus.com/wp-content/uploads/2019/01/b200-b210_spec_sheet.pdf, 2019. Accessed: 2024-12-10.

[62] Signal Hound. Bb60c signal analyzer. https://signalhound.com/sigdownloads/datasheets/Signal-Hound-BB60C-Data-Sheet.pdf, 2023. Accessed: 2024-12-10.

[63] Mini-Circuits. ZN2PD2-63-S+ Datasheet, Accessed 2025. Last accessed: March 19, 2025.

[64] Texas Instruments. Opa330 operational amplifier. https://www.ti.com/product/OPA330. Accessed: 2024-12-09.

[65] Aaron N. Parks, Angli Liu, Shyamnath Gollakota, and Joshua R. Smith. Turbocharging ambient backscatter communication. In *Proceedings of the 2014 ACM Conference on SIGCOMM*, SIGCOMM '14, page 619–630, New York, NY, USA, 2014. Association for Computing Machinery.

[66] STMicroelectronics. Ts881 operational amplifier. https://www.st.com/resource/en/datasheet/ts881.pdf. Accessed: 2024-12-09.

[67] Diodes Incorporated. 1n5817-1n5819 schottky barrier rectifiers. https://www.diodes.com/assets/Datasheets/1N5817-1N5819.pdf. Accessed: 2024-12-09.

[68] Ettus Research. Vert900 vertical antenna. https://www.ettus.com/all-products/vert900/. Accessed: 2024-12-01.

[69] Digilent. Analog discovery 3 reference manual, 2024. Accessed: March 26, 2025.

[70] Michael Buettner, Richa Prasad, Matthai Philipose, and David Wetherall. Recognizing daily activities with rfid-based sensors. In *Proceedings of the 11th International Conference on Ubiquitous Computing*, UbiComp '09, pages 51–60, New York, NY, USA, 2009. ACM.

[71] Daniel J Yeager et al. Neuralwisp: A wirelessly powered neural interface with 1-m range. *IEEE Transactions on Biomedical Circuits and Systems*, 2009.

[72] Hong Zhang et al. Moo: A batteryless computational rfid and sensing platform. 2011.

[73] Federal Communications Commission. Title 47 CFR Part 15 - Radio Frequency Devices, 2025. Accessed: March 26, 2025.

[74] International Telecommunication Union. Itu-r recommendation p.1411-12: Propagation data and prediction methods for the planning of short-range outdoor radiocommunication systems and radio local area networks in the frequency range 300 mhz to 100 ghz. https://www.itu.int/dms_pubrec/itu-r/rec/p/R-REC-P.1411-12-202308-I!!PDF-E.pdf, 2023. Accessed: 2024-11-22.

[75] P. Massoud Salehi and J. Proakis. *Digital Communications*. McGraw-Hill Education, 2007.

[76] Nakul Garg and Nirupam Roy. Sirius: A self-localization system for resource-constrained iot sensors. In *Proceedings of the 21st Annual International Conference on Mobile Systems, Applications and Services*, MobiSys '23, page 289–302, New York, NY, USA, 2023. Association for Computing Machinery.

[77] Bryce Kellogg, Vamsi Talla, and Shyamnath Gollakota. Bringing gesture recognition to all devices. In *Proceedings of the 11th USENIX Conference on Networked Systems Design and Implementation*, NSDI'14, page 303–316, USA, 2014. USENIX Association.

[78] Ajibayo O. Adeyeye, Charles Lynch, Aline Eid, Jimmy G. D. Hester, and Manos M. Tentzeris. Energy autonomous two-way repeater system for non-line-of-sight interrogation in next generation wireless sensor networks. *IEEE Transactions on Microwave Theory and Techniques*, 70(3):1779–1788, 2022.

[79] C. Rajashekar Reddy, Manoj Gulati, and Ambuj Varshney. Beyond broadcasting: Revisiting fm frequency-band for providing connectivity to next billion devices. In *Proceedings of the 11th International Workshop on Energy Harvesting & Energy-Neutral Sensing Systems*, ENSsys '23, page 30–36, New York, NY, USA, 2023. Association for Computing Machinery.